



Cite this: *Nanoscale*, 2020, **12**, 22787

The development of an antifouling interpenetrating polymer network hydrogel film for salivary glucose monitoring†

Zifeng Zhang,^{a,b} Qian Dou,^{a,b} Shiwen Wang,^b Debo Hu,^{b,c} Bei Yang,^{b,c} Zhipeng Zhao,^{b,c} Hongliang Liu^{id}*^d and Qing Dai^{id}*^{a,b,c}

Owing to its rapid response and broad detection range, a phenylboronic acid (PBA)-functionalized hydrogel film-coated quartz crystal microbalance (QCM) sensor is used to non-invasively monitor salivary glucose in diabetic patients. However, nonspecific protein adsorption on the PBA-functionalized hydrogel film can cause dramatic loss of sensitivity and accuracy of the sensor. A traditional zwitterionic polymer surface with ultra-low protein fouling can hinder the interaction of PBA in the hydrogel matrix with glucose molecules owing to its steric hindrance, resulting in poor glucose sensitivity of the sensor. Herein, we developed a novel hydrogel film that enhanced the antifouling properties and sensitivity of the QCM sensor by infiltrating a glucose-sensitive monomer (*i.e.*, PBA) into a zwitterionic polymer brush matrix to form an interpenetrating polymer network (IPN). The IPN hydrogel film could minimize the glucose sensitivity loss since the antifouling polymer distributed in its matrix. Moreover, a stable hydration layer was formed in this film that could prevent water from transporting out of the matrix, thus further improving its antifouling properties and glucose sensitivity. The experimental results confirmed that the IPN hydrogel film possessed excellent resistance to protein fouling by mucin from whole saliva with reductions in adsorption of nearly 88% and could also enhance the glucose sensitivity by nearly 2 fold, compared to the PBA-functionalized hydrogel film. Therefore, the IPN hydrogel film provides improved antifouling properties and sensitivity of the QCM sensor, which paves the way for non-invasive monitoring of low concentrations of glucose in saliva.

Received 8th August 2020,
Accepted 8th October 2020

DOI: 10.1039/d0nr05854h

rsc.li/nanoscale

Introduction

Saliva is an ideal medium for non-invasive glucose monitoring, since its collection procedure is harmless and convenient and can be done in real time.^{1–6} However, the concentration of glucose in saliva is only 1 to 10% of that in the blood, which is considered very low; thus, the monitoring of such a low concentration of glucose requires a highly sensitive biosensor.⁷ Quartz crystal microbalance (QCM) is a mass-sensitive biosensor that has high sensitivity, fast response, low-cost pro-

duction, capability of real-time measurement and simple integration; it can detect the changes of mass at the sub-nano gram level.^{8–15} Various studies have indicated that sensing materials are key factors to affect the properties of the QCM sensor including sensitivity and response time. For example, Li *et al.*¹⁶ have prepared a glucose-sensitive QCM sensor based on a self-assembled monolayer film of cyclic peptides. They found that the frequency shift increases with an increase in glucose concentration from 1.8 to 3600 mg L⁻¹; however, the response time was 30 min owing to slow response kinetics. As a consequence, Dou *et al.*¹⁷ have reported a glucose-sensitive QCM sensor based on a phenylboronic acid (PBA)-functionalized hydrogel film, which has a detection range of 10 mg L⁻¹–5000 mg L⁻¹ and a response time of 100 s. Although the film-coated QCM sensor has high performance, the film material is not resistant to non-specific protein adsorption, an event that can cause losses of sensitivity and accuracy of the sensor, thus limiting its practical application in salivary glucose monitoring.^{18–23}

In efforts to prevent nonspecific protein adsorption, many researchers have studied the mechanisms of protein resistance, from which they found that the stability of the hydration layer is the key factor that determines the protein-resistant properties.²⁴ For example, the ionic solvation-based zwitterionic

^aSchool of Materials Science and Engineering, Zhengzhou University, Zhengzhou 450001, P. R. China

^bDivision of Nanophotonics, CAS Key Laboratory of Standardization and Measurement for Nanotechnology, CAS Center for Excellence in Nanoscience, National Center for Nanoscience and Technology, Beijing 100190, P. R. China. E-mail: daiq@nanoctr.cn

^cCenter of Materials School and Optoelectronics, University of Chinese Academy of Sciences, Beijing 100049, P. R. China

^dTechnical Institute of Physics and Chemistry, University of Chinese Academy of Sciences, Beijing 100190, P. R. China. E-mail: liuhl@mail.ipc.ac.cn;

Tel: +86-010-82545720

†Electronic supplementary information (ESI) available. See DOI: 10.1039/d0nr05854h

polymer often has a better protein resistance than hydrogen bonding-based polyethylene glycol (PEG). This is attributed to the fact that the ionic solvation-based antifouling zwitterionic polymer can bind to more water molecules and can bind more tightly compared to hydrogen bonding-based PEG, thus resulting in a more stable hydration layer.²⁵ Currently, the most widely studied antifouling zwitterionic polymers include zwitterionic hydrogel and zwitterionic polymer brushes. The zwitterionic hydrogel is often prepared by copolymerizing a zwitterionic monomer and a glucose-sensitive monomer (e.g., PBA) to improve the protein resistance of the PBA-functionalized hydrogel film. However, the structure of the hydrophilic crosslinker used for preparing the PBA-functionalized hydrogel is different from that of the zwitterionic monomer, thus disrupting the stability of the hydration layer of the zwitterionic hydrogel.²⁶ Recently, to obtain the stable hydration layer, film surfaces have been functionalized with zwitterionic polymer brushes (traditional antifouling coating) *via* surface-initiated atom transfer radical polymerization (ATRP). The obtained zwitterionic polymer surfaces can reduce the adsorption of nonspecific protein in undiluted bovine serum by over 99%.^{27,28} However, the transport of glucose molecules can be impeded by traditional antifouling coating due to its steric hindrance.^{29–32} This results in poor glucose sensitivity of the PBA-functionalized hydrogel film-coated sensor, thus limiting its application in the detection of low salivary glucose levels. Therefore, the key challenge for salivary glucose monitoring is to obtain a PBA-functionalized hydrogel film that has a stable hydration layer so that it has dual-functional properties including high protein resistance and high glucose sensitivity.

An interpenetrating polymer network (IPN) is often used in polymer science to produce materials that have dual-functional properties (such as antifouling and mechanical properties) due to its advantages such as high entanglement and favorable interaction between network components.^{33–35} However, most of the antifouling IPN hydrogels reported in the literature utilized a synthetic polymer (e.g., PEG) as an antifouling component, in which case, chemicals such as those that contain methacrylate groups are required to modify and photo-crosslink the polymers. This has complicated the synthesis of IPN hydrogels. Moreover, PEG is prone to oxidative degradation, thus destabilizing the hydration layer.^{36,37}

To provide a stable hydration layer for the PBA-functionalized hydrogel film, a facile two-step method of synthesizing the IPN hydrogel film is reported in this work. First, polySBMA brushes with different lengths were attached to the surface of a quartz chip *via* surface-initiated ATRP. Surface-initiated ATRP enables the synthesized zwitterionic polymer brushes with high surface density and controllable thickness, thus achieving a stable hydration layer.^{38–45} Then, a mixture of glucose-sensitive PBA, acrylamide (AM), and crosslinker (MBAA) was incorporated into the polySBMA brush matrix. The incorporation was accomplished *via* the UV gel curing process. The IPN hydrogel film can achieve excellent glucose sensitivity and protein-resistant properties, which is mainly attributed to high entanglement and favorable interaction between the antifoul-

ing polySBMA brushes and the glucose-sensitive hydrogel and the presence of the stable hydrogel layer in its matrix instead of its surface. The protein resistance and glucose sensitivity of the IPN hydrogel film were optimized by varying the thicknesses of the polySBMA brushes. We found that with polySBMA at a thickness of ~50 nm, the IPN hydrogel film could significantly reduce the nonspecific protein adsorption and detect salivary glucose in the typical concentration range (0–50 mg L⁻¹). Therefore, this study presents a new strategy for improving the antifouling properties and sensitivity of glucose sensors.

Results and discussion

Synthesis and structure of the IPN hydrogel film

Fig. 1a demonstrates the immobilization of the IPN hydrogel film onto a quartz chip *via* a facile two-step method. Briefly, the quartz chip was first cleaned with Piranha solution to eliminate organic substances. The initiator was attached to the quartz chip through bifunctional molecules, which contained an ATRP initiator at one end (a bromoisobutyrate moiety) and a thiol at the other end, the feature that allows one-step functionalization of the surface of the quartz chip with the MUBiB initiator by forming an alkanethiol SAM. The MUBiB chains attached to the gold substrate (quartz chip) contain $-C(CH_3)_2Br$ groups, which serve as initiating sites in subsequent ATRP for the preparation of polySBMA brushes.⁴⁶ In the subsequent ATRP, SBMA was utilized as a monomer to generate polySBMA brushes that were then coated onto the quartz chip (Fig. 1a-i). Finally, the prepolymer solution consisting of AM, PBA and Bis was incorporated into the polySBMA brush matrix by which the polySBMA brush matrix was immersed in the prepolymer solution for 30 min and was then spin-coated to form a homogeneous liquid layer. The IPN hydrogel film was synthesized using the UV gel curing process (Fig. 1a-ii).

As illustrated in Fig. 1b, the change in frequency shift was not obvious, when the glucose solution was pumped into the pSBMA coating modified PBA-functionalized hydrogel film, indicating that the pSBMA coating can cause the reduction in the glucose sensitivity of the PBA-functionalized hydrogel film, making it unsuitable for monitoring low salivary glucose levels. This may be attributed to the steric hindrance caused by pSBMA coating. Similar results were also demonstrated by Ingber *et al.*, in which they found that traditional antifouling coating could also hinder electron transfer, resulting in poor sensitivity.³² To address this drawback, the IPN hydrogel film was fabricated in this work; and to avoid the effect of film thickness on glucose sensitivity, the thickness of the PBA-functionalized hydrogel film and the IPN hydrogel film was chosen as 438 nm and 440 nm, respectively (Fig. S1 and S2†). Fig. 1b shows that at a similar thickness, the glucose sensitivity of the IPN hydrogel film was nearly 2-fold as high as that of the PBA-functionalized hydrogel film. The possible mechanism of glucose sensitivity and protein resistance of the hydrogel film, which could be either through hydrogen bonding or ionic sol-

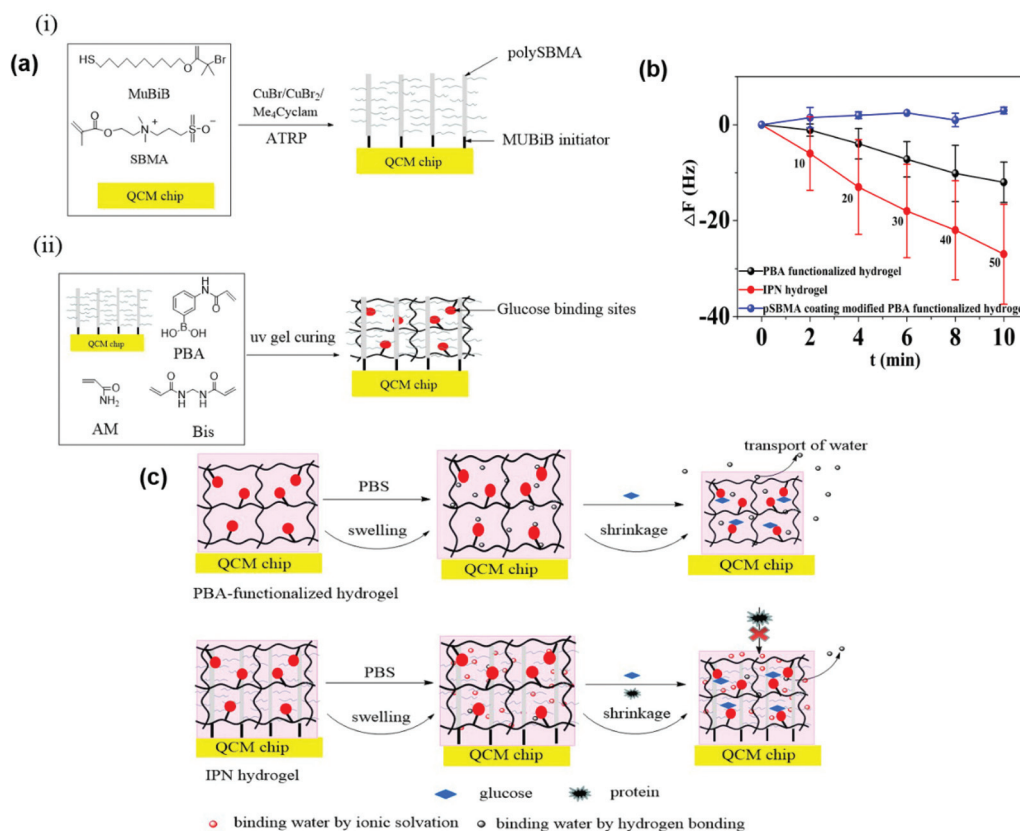


Fig. 1 (a) Schematic diagram showing the synthesis procedure for the IPN hydrogel film: the quartz chip was coated with polySBMA brushes (i) and then coated with the IPN hydrogel film (ii). (b) Sensitivity to glucose of the PBA-functionalized hydrogel film, the IPN hydrogel film at thicknesses of 438 nm and 440 nm, and the pSBMA coating modified PBA-functionalized hydrogel film. Numbers shown in the graph represent the glucose level. (c) A schematic diagram illustrating the protein resistance of the IPN hydrogel film and the binding of the PBA-functionalized hydrogel film and the IPN hydrogel film to glucose.

vation, is shown in Fig. 1c. Whereas the PBA-functionalized hydrogel film forms unstable hydration layers *via* hydrogen bonds, the IPN hydrogel film forms more stable hydration layers *via* ionic solvation, which are caused by the strong hydration capacity of pSBMA brushes. Fig. 1c shows that the interaction of the PBA-functionalized hydrogel film with glucose caused volumetric shrinkage; as a result, water could be transported to the outside of the hydrogel matrix causing water loss.⁴⁷ This water loss resulted in an additional hydrogel mass loss, which in turn reduced the glucose sensitivity of QCM. Compared with that of the PBA-functionalized hydrogel film, the interaction of the IPN hydrogel film with glucose caused smaller volumetric shrinkage due to stable hydrated layers formed by ionic solvation; therefore, the transport of water to the outside of the IPN hydrogel film was nearly unobservable. The effect of the transport of water on glucose sensitivity has also been demonstrated in our recent work.⁴⁸ Owing to its advantages, such as high entanglement and favorable interaction between network components, the IPN hydrogel film has dual-functional properties, which are antifouling and glucose sensitivity. Owing to their strong hydration capacity caused by ionic solvation, the polySBMA brushes that are

coated on the quartz chips are highly resistant to bacterial adhesion and biofilm formation.²⁵ Moreover, with antifouling polySBMA brushes distributed in its matrix instead of its surface, the IPN hydrogel film can minimize the glucose sensitivity loss. For these reasons, the IPN hydrogel film had higher glucose sensitivity and protein resistance.

Characterization of the IPN hydrogel film

FTIR was employed to characterize the chemical reaction occurring at the surface of the quartz chip during each step of the IPN hydrogel film synthesis process (Fig. 2a). Before attaching an initiator to the quartz chip, the IR spectrum of the acid-treated quartz chip was not obvious (Fig. 2a-I). After the introduction of the MUBiB initiator on the quartz chip, the characteristic peaks corresponding to the stretching and bending vibration of C–H in $-\text{CH}_2$ simultaneously appeared at 2926, 2846, and 1461 cm^{-1} , which indicates that the SAM formed using an initiator has been attached to the surface of the quartz chip (Fig. 2a-II). The characteristic peak of C–Br was almost unobservable, because the SAM on the surfaces was very thin.⁴⁹ Bands at 1040 and 1181 cm^{-1} are attributed to the symmetric and asymmetric stretching vibration of S=O

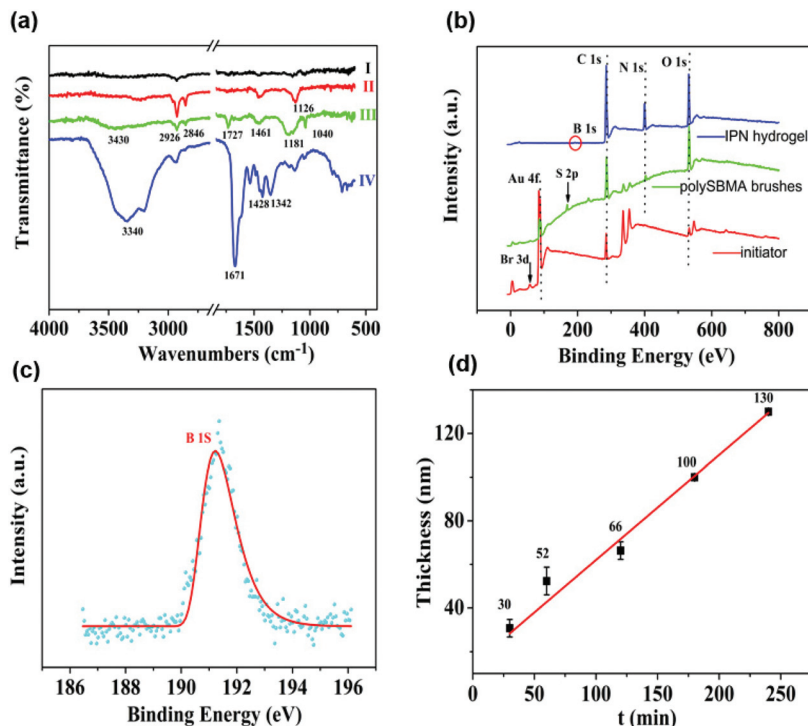


Fig. 2 (a) FTIR spectra of: (I) the quartz chip cleaned with Piranha solution; (II) the quartz chip coated with the initiator; (III) the quartz chip coated with polySBMA brushes; and (IV) the quartz chip coated with the IPN hydrogel film. (b) XPS spectra of the quartz chip coated with the initiator, polySBMA brushes, and IPN hydrogel film. (c) An enlarged image of the area in the red circle shown in (b). (d) Change in polySBMA brush thickness with polymerization time; the reaction was carried out in ethanol/water solution at 30 °C.

groups, respectively, and those at 1727 and 3430 cm⁻¹ are attributed to the stretching vibration of C=O in -COOC and of O-H, respectively. This demonstrates that the polySBMA brushes were successfully attached to the quartz chip (Fig. 2a-III). Finally, the characteristic peak of -B(OH)₂ was observed at 1342 cm⁻¹, indicating that the PBA-functionalized hydrogel was successfully deposited into the polySBMA brushes (Fig. 2a-IV).

To further examine the surface properties of the IPN hydrogel film during each step of its synthesis process, XPS was employed to track the change in the surface composition of the initiator on the quartz chip, as well as that of the polySBMA brushes and IPN hydrogel film that were coated on the quartz chip. The detailed XPS data of different samples can be found in Table S1.† According to the data, after the first step of the reaction, which took place for 24 h, a small amount of bromine (0.194%, Br_{3d}) appeared at the binding energy of about 69 eV (Fig. 2b). This further indicates that the initiator was successfully attached to the surface of the quartz chip. After the reaction with the surface-initiated ATRP, the characteristic signal of bromine disappeared, while that of sulfo-betaine (S_{2p} at 167 eV, N_{1s} at 402 eV) appeared, indicating that the polySBMA brushes were successfully grown from the surface of the quartz chip. Some researchers suggested that the disappearance of the bromine signal may be due to the termination of some living chains.⁴² However, other researchers

believed that the XPS method can only measure to a depth of ~10 nm, and the chains on the surface may be entangled; thus, the end of the living chains may not be located in the outermost layer of the surface.⁵⁰ The presence of the boric acid derivative was confirmed by the high-resolution scanning spectrum of B_{1s} located at 191 eV (Fig. 2c). These results indicate that the IPN hydrogel film has been successfully prepared. As shown in Fig. 2d, the thickness of polySBMA brushes linearly increased with an increase in polymerization time and was the highest with a value of 130 nm when the polymerization time was about 4 h. These results suggest that it is possible to control the thickness of polySBMA brushes using surface-initiated ATRP.

The surface roughness of the IPN hydrogel film

The effects of the SAM, polySBMA brushes and IPN hydrogel film on the surface roughness of the quartz chip were examined using AFM. As shown in Fig. 3, compared with that of the unmodified quartz chip ($R_{ms} = 7.53$ nm, Fig. 3a), the surface roughness of the SAM-coated quartz chip was lower ($R_{ms} = 7.47$ nm, Fig. 3b), which might be due to the fact that the SAM was very thin and homogeneous. In addition, the surface roughness of the polySBMA brush-coated quartz chip ($R_{ms} = 5.80$ nm) was lower than that of the SAM-coated quartz chip by 22%, indicating that homogeneous polySBMA brushes were formed (Fig. 3c). The homogeneous polySBMA brushes can

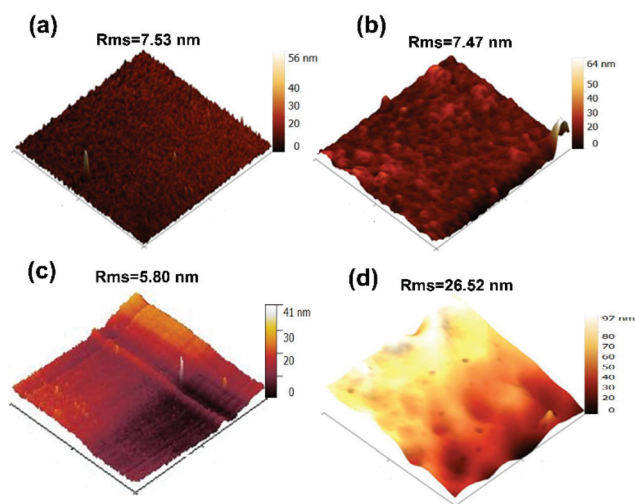


Fig. 3 AFM images of: (a) the uncoated quartz chip; (b) the SAM-coated quartz chip; (c) the polySBMA brush-coated quartz chip; and (d) the IPN hydrogel film-coated quartz chip. Different colors indicate different film thickness.

achieve exceptional resistance to protein adsorption, presumably because these brushes present a high-enough surface density of SBMA moieties at the solid/water interface to prevent the adsorption of proteins.¹⁸ The surface roughness of the polySBMA brush-coated quartz chip increased ($R_{\text{ms}} = 26.52$ nm) after the pre-polymer solution consisting of the glucose-sensitive monomer was incorporated into the polySBMA brushes (Fig. 3d). This further demonstrated that the PBA-functionalized hydrogel has been successfully incorporated into the polySBMA brush matrix. This is consistent with the observations by Beek *et al.*,⁵¹ in which they have observed that the incorporation of a small amount of hyaluronic acid into pHEMA hydrogels can increase the surface roughness.

Glucose sensitivity and protein resistance of the IPN hydrogel film in PBS solution

Phenylboronic acid (PBA) exists in two forms in aqueous solution, namely in a negatively charged dissociated state and in an uncharged non-dissociated state. Dissociation equilibrium exists between these two states. Non-dissociated PBA is a flat triangle and forms an unstable complex with glucose, while dissociated PBA has a tetrahedral structure and can form cyclic lactones with glucose molecules *via* the reversible interaction of diol-containing glucose molecules and the hydroxyl group of dissociated PBA (see Fig. S3†).^{52–54} The QCM technique is a mass sensitive tool which utilizes the piezoelectric properties of quartz crystals to measure the attached mass on the quartz surface. When voltage is applied to a quartz crystal causing it to oscillate at a specific frequency, the change in mass on the quartz surface is related to the change in frequency of the oscillating crystal. As shown in Fig. S4a,† there is no increase in frequency shift when glucose molecules

cannot be specifically recognized by the IPN hydrogel film without PBA. However, when PBA is introduced to the IPN hydrogel film, it can effectively recognize the glucose molecules, causing an obvious increase in frequency shift (Fig. S4b†). Fig. S5† shows that the QCM sensor based on the IPN hydrogel film reveals little fluctuation in frequency shifts (3.1 Hz, the fundamental frequency of this QCM system is 5×10^6 Hz, only 0.62 millionth of the fundamental frequency) over 240 min in pH = 7.5 PBS solution. This demonstrates that the IPN hydrogel film-coated QCM sensor has good stability. In our recent work, we have demonstrated that the hybrid hydrogel film-coated QCM sensor possessed a similar stability.⁴⁸ Briefly, the total content of proteins in saliva is about $71\text{--}2232$ mg L⁻¹, of which the content of Muc. is 1190 ± 170 mg L⁻¹.⁵⁵ To adjust the pH of the sample solution, the sample solutions consisting of the pH = 7.5 PBS/saliva mixture (1 : 1 v/v) were used in the QCM test in this study. As a result, the concentration of protein in saliva could be diluted twice as much. Therefore, 500 mg L⁻¹ Muc., 500 mg L⁻¹ BSA and 500 mg L⁻¹ Fib. were used in QCM tests to study the protein-resistant properties of the IPN hydrogel film. As can be seen in Fig. 4a, at thicknesses greater than 52 nm, the frequency shift increased with an increase in the thickness of polySBMA brushes. The increase in the frequency shift of the sensor indicated an increase in mass on the surface, which was physically correlated with the increase in the mass of protein vibrating with the sensor.⁵⁶ This may be because a thick polySBMA brush layer could lead to strong dipole interactions between zwitterionic pairs, thus reducing the hydration of the brush and causing protein adsorption.²⁸ A positive frequency shift was observed at a thickness greater than 52 nm. A similar result was also reported by Healy *et al.*,⁵⁷ in which they observed a positive frequency shift when 300 mg L⁻¹ Fib. was adsorbed onto the IPN film surface. They described that this is due to the fact that the viscosity and density of the bulk fluid was changed compared to those of PBS. The response to 10 mg L⁻¹ glucose of the IPN hydrogel film containing polySBMA brushes with different thicknesses is shown in Fig. 4b. A positive change in frequency shift was also observed for the IPN hydrogel film containing polySBMA brushes with thicknesses of ≥ 62 nm, unlike thin polySBMA brushes. In general, a negative frequency shift should be observed when the glucose molecules were adsorbed onto the IPN hydrogel film-coated QCM sensor. Thus, this unexpected positive frequency shift may be attributed to the transport of water molecules to the exterior of the IPN hydrogel film, causing the mass of the sensing layer to decrease. In our recent work, we have demonstrated that poor viscoelasticity of the PBA-functionalized hydrogel film leads to the transport of water to the outside of the hydrogel matrix owing to the increased cross-linking density by glucose recognition.⁴⁸ The curing reactions of the IPN hydrogel film may be hampered by the steric hindrance of the interlocking network of thick polySBMA brushes, causing poor viscoelasticity. Similar observations have also been reported by Lee *et al.*⁵⁸ Therefore, to obtain the IPN hydrogel film with high glucose sensitivity and protein resis-

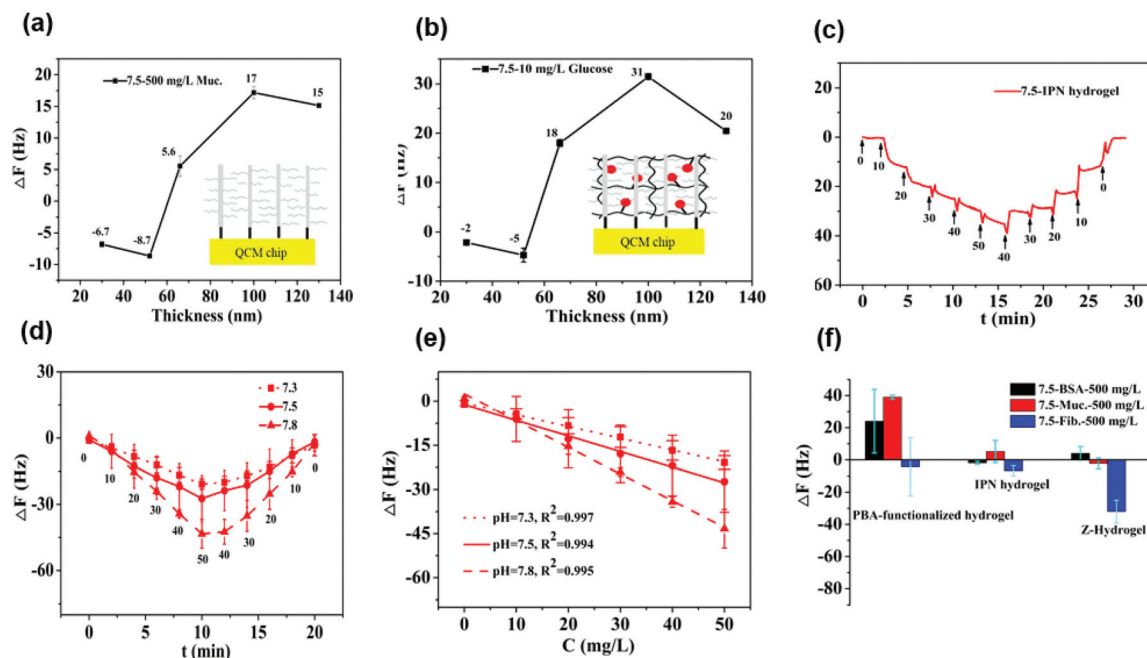


Fig. 4 (a) Adsorption of Muc. (500 mg L^{-1}) on polySBMA brushes with different thicknesses. (b) Response to glucose (10 mg L^{-1}) of the IPN hydrogel film formed with polySBMA brushes with different thicknesses at $\text{pH} = 7.5$. The numbers in (a) and (b) represent the frequency shift. (c) Response and recovery of the IPN hydrogel film measured using a QCM sensor at $\text{pH} = 7.5$. (d) Response and recovery of the IPN hydrogel film at different pH values. The numbers in (c) and (d) represent the glucose level. (e) Relationship between frequency shift and glucose concentration. (f) Adsorption of 500 mg L^{-1} BSA, 500 mg L^{-1} Muc., and 500 mg L^{-1} Fib. on the PBA-functionalized hydrogel film, the IPN hydrogel film, and the z-hydrogel film at $\text{pH} = 7.5$. The z-hydrogel represents the zwitterionic hydrogel.

tance, the polymerization time of polySBMA brushes was chosen as 1 h.

We further studied the effect of the thickness of the IPN hydrogel film on their glucose sensitivity and protein resistance. The different thicknesses of the film (such as 360, 420, 440, and 630 nm) were prepared, and the results can be found in Fig. S1.† According to the results, the thickness at a certain range had no obvious effect on the protein-resistant properties of the IPN hydrogel film (Fig. S6a†). This is mainly attributed to the strong hydration capacity of polySBMA brushes caused by ionic solvation. The relationship between the thickness of the IPN hydrogel film and the frequency shift of glucose sensitivity (data can be found in Fig. S6b†) showed that the frequency shift increased as the film thickness increased from 360 nm to 440 nm. This is likely due to the fact that the thicker the IPN hydrogel film, the more glucose molecules it can bind.⁵⁹ Nonetheless, the IPN hydrogel film with a thickness of 630 nm had poor glucose sensitivity. A similar result has also been observed by Dou *et al.*⁶⁰ In their study, they demonstrated that the thickness of the PBA-functionalized hydrogel film has a significant effect on its glucose sensitivity, and the hydrogel film with a thickness of 600 nm has poor glucose sensitivity due to its poor viscoelasticity. Therefore, the thickness of the IPN hydrogel film was selected as 440 nm in this work.

The concentration of glucose in saliva is only 1 to 10% of that in blood, and the typical salivary glucose level in humans

is between 0.54 mg L^{-1} and 37.8 mg L^{-1} .⁷ Therefore, the glucose concentrations of $0\text{--}50 \text{ mg L}^{-1}$ were selected in this study to study the glucose sensitivity. The response and recovery behavior are important parameters for evaluating the dynamic performance of the QCM glucose sensor. Fig. 4c shows the response of the IPN hydrogel film to glucose at the concentration range of 0.0 to 50 mg L^{-1} . When glucose with increasing concentration was pumped into the flow cell, the fundamental frequency of the IPN hydrogel film-coated quartz chip decreased due to the binding of glucose with the IPN hydrogel film. In contrast, when glucose with decreasing glucose concentration was pumped, the fundamental frequency increased, reaching the maximum value (the value of glucose-free solution), due to the dissociation of glucose from the IPN hydrogel film. These results indicate that the dynamic range of the IPN hydrogel film-coated QCM sensor is broad enough to cover the typical range of salivary glucose. The binding of glucose with boronic acid in the IPN hydrogel film is pH dependent; thus, we conducted another glucose detection experiment at different pH values from 7.3 to 7.8 (Fig. 4d). According to the data, glucose concentration was linearly correlated with pH (Fig. 4e), and the highest glucose sensitivity was observed at $\text{pH} = 7.8$. This is likely due to the fact that a higher pH value can facilitate the binding between glucose and boronic acid in the IPN hydrogel film. However, there was a slight lag of glucose desorption at this pH ($\text{pH} = 7.8$), which may be attributed to the variations in the network stress of the

IPN hydrogel film derived from the swelling effect at high pH values.⁶¹ Therefore, based on these results, it can be inferred that the optimal pH that results in the excellent glucose sensitivity and dynamic performance of the IPN hydrogel film-coated QCM sensor is pH = 7.5. The adsorption of BSA, Muc. or Fib. onto the hydrogel film, the IPN hydrogel film and the z-hydrogel film was measured by QCM (Fig. 4f). The IPN hydrogel film reduced the adsorption of Muc. by about 88% compared with that of the PBA-functionalized hydrogel film, indicating that the IPN hydrogel film has excellent protein resistance. To study the effect of hydration layers on protein resistance, the z-hydrogel film was prepared. The z-hydrogel film could largely increase the adsorption of Fib., which further demonstrated that the hydrophilic crosslinker (Bis) could not suitably crosslink the zwitterionic polymer, causing it to have unstable hydration layers.²⁶ In general, to confirm the repeatability of the sensors, three cycles of testing are needed.⁶² Therefore, five cycles of testing were selected in this study. In the present study, repeatability testing was performed by alternatively pumping PBS solution (pH = 7.5, glucose-free) and glucose solution (10, 30 and 50 mg L⁻¹) into the flow cell. As illustrated by Fig. S7,[†] the IPN hydrogel film still has high sensitivity to glucose under various concentrations after five association–dissociation cycles. Moreover, as listed in Table S2,[†] the relative standard deviations (% RSD) of the QCM frequency response for this IPN hydrogel film at glucose concentrations of 10, 30 and 50 mg L⁻¹ are 2.4%, 8.3% and 6.5% ($n = 5$) respectively. Currently, blood glucose sensor variances in the United States typically range from 3 to 10% for

disposable and continuous monitoring systems.⁶³ Thus, these results demonstrate that the IPN hydrogel film has an acceptable repeatability. The response to interferences such as fructose was not tested in this study, and this is because there are almost no other saccharides except for glucose in saliva.⁵⁵ Moreover, in a recent study by Dou *et al.*,¹⁷ which investigated the influence of possible competitive binding of interferences (0.1 mM) on the glucose detection, it is demonstrated that the PBA-functionalized hydrogel film-coated QCM sensor can effectively detect glucose, despite the presence of other saccharides, such as fructose, maltose, and lactose.

The glucose sensitivity and protein resistance of the IPN hydrogel film in saliva

Saliva contains different types of molecules, such as ions, low molecular weight organic substrates, and proteins, which have adverse effects on the sensitivity and accuracy of the detection using the QCM sensor. Therefore, the PVDF film, solid phase extraction, 100 °C for 30 min and an ion exchange resin were employed to remove most of these molecules from saliva prior to the detection.⁶⁴ To evaluate the sensitivity of the IPN hydrogel film in response to glucose in real human saliva, a moderate amount of glucose was spiked into the saliva. Fig. 5a and b show the response and recovery of glucose in diluted saliva ($V_{7.5\text{PBS}} : V_{\text{saliva}} = 9 : 1$) using the IPN hydrogel film-coated and PBA-functionalized hydrogel film-coated QCM sensor. At 10 mg L⁻¹ glucose, the frequency shift of the IPN hydrogel film was 28 Hz, which is a reduction by about 83% compared with

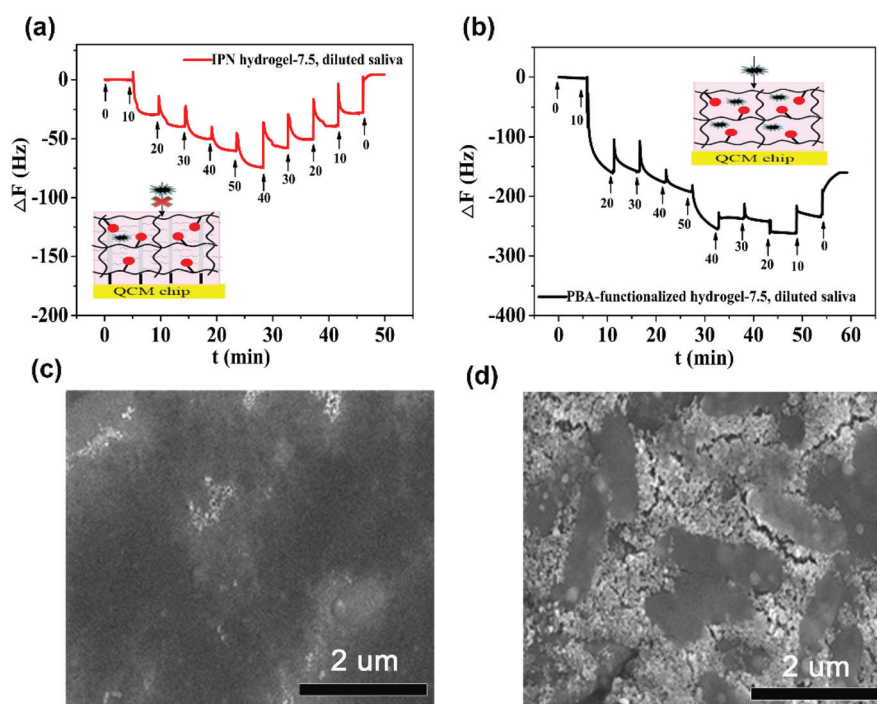


Fig. 5 (a and b) Response and recovery of glucose in diluted saliva by (a) the IPN hydrogel film and (b) the PBA-functionalized hydrogel film. The numbers in (a) and (b) represent the spiked glucose level. (c–d) SEM images of (c) the IPN hydrogel film and (d) the PBA-functionalized hydrogel film after 48 h incubation with human saliva.

that of the PBA-functionalized hydrogel film (frequency shift: 163 Hz).

This indicates that the IPN hydrogel film possesses excellent resistance to nonspecific protein adsorption in diluted saliva, compared to the PBA-functionalized hydrogel film. Moreover, a severe lag of glucose desorption was observed in the PBA-functionalized hydrogel film, possibly caused by the nonspecific protein adsorption.⁶⁵ To further confirm the protein-resistant properties of the IPN hydrogel film, we carried out SEM imaging of the IPN hydrogel film and the PBA-functionalized hydrogel film after incubating with human saliva for 48 h, and the results are shown in Fig. 5c and d. As can be seen from Fig. 5d, various impurities (*e.g.*, protein and bacteria) were found adhered onto the PBA-functionalized hydrogel film surface, as was also observed by the large frequency shift of the hydrogel in diluted saliva. By contrast, impurities on the IPN hydrogel film surface were nearly unobservable (Fig. 5c), suggesting that the IPN hydrogel has good protein resistant properties, thus avoiding nonspecific adsorption. The response and recovery of glucose in diluted saliva by the IPN hydrogel film had good linearity with $R^2 = 0.952$ and 0.949 , respectively. The glucose level in diluted saliva calculated based on the response and recovery curves can be found in Fig. S8.† The total content of proteins in the serum is about 6×10^4 – 8×10^4 mg L⁻¹, which is 27–1100 fold higher than that in saliva (72 – 2232 mg L⁻¹).⁵⁵ Therefore, to minimize the nonspecific protein adsorption, a moderate amount of glucose was spiked into 1% diluted serum ($V_{7.5\text{PBS}} : V_{\text{serum}} = 99 : 1$). The PVDF film and ion exchange resin were also employed to remove most of these molecules from the serum prior to the detection. Fig. S9a† shows the detection of glucose in the diluted serum using the IPN hydrogel film-coated QCM sensor. As the glucose concentrations gradually increased, the frequency shift became more negative. Moreover, a frequency shift of 45 Hz was observed due to nonspecific protein adsorption, when the diluted serum (glucose-free solution) was pumped into the flow cell. However, unlike the PBA-functionalized hydrogel film-coated QCM sensor ($R^2 = 0.713$, see Fig. S10†), the nonspecific protein adsorption does not affect the glucose detection of the proposed QCM sensor, because the glucose concentration had a good linear relationship with frequency shift ($R^2 = 0.978$, see Fig. S9b†). These results demonstrate that the IPN hydrogel film can potentially be applied to detect glucose in complex biological samples such as saliva and serum. To embody the advantage of the QCM glucose sensor, the analytical properties of the QCM sensor were compared with other detection methods. The results are summarized in Table S3.† Obviously, the advantages of glucose monitoring by using the QCM sensor are the IPN hydrogel film with excellent antifouling properties, glucose sensitivity and simple storage conditions over other detection methods like electrochemical sensors. Likewise, to enhance the accuracy of glucose detection in saliva or serum samples using the proposed QCM sensor, the samples need a complex processing process to remove proteins, *etc.* The detailed discussion can be found in the ESI.†

Experimental

Materials

Fibrinogen, fraction I from bovine plasma (Fib.), Amberlite 732 and Amberlite IRA-4200 were purchased from Macklin. Mucin (Muc.) from the bovine submaxillary gland was purchased from Shanghai Yuanye Biotechnology Co. Ltd. Bovine serum albumin (BSA), copper(i) bromide (99%), copper(ii) bromide (99%), Me₄Cyclam (98%), 0.2 μm PVDF blotting films and cattle serum were obtained from Sigma-Aldrich. *N*-(3-Sulfopropyl)-*N*-(methacryloxyethyl)-*N,N*-dimethylammonium betaine (SBMA, 99%) and 2-hydroxy-2-methylpropiophenone (HMPP, 99%) were purchased from J&k. ω-Mercaptoundecyl bromoisobutyrate (MUBiB, ≥95%) was obtained from Shanghai D&B Biological Science Technology Co. Ltd. *N,N*-Methylenebisacrylamide (Bis, 98%) was purchased from Sinopharm Chemical Reagent Co. Ltd. 3-Acrylamidophenylboronic acid (PBA, 98%) was obtained from Ark Pharm. Acrylamide (AM, 98.5%) was purchased from Xilong Chemical Industry. Sulfuric acid (H₂SO₄, AR), hydrogen peroxide (H₂O₂, 30% aqueous solution), ethanol (C₂H₅OH, AR), dimethyl sulfoxide (DMSO, AR), glucose (C₆H₁₂O₆, AR), sodium phosphate dibasic dodecahydrate (Na₂HPO₄, AR) and potassium dihydrogen phosphate (KH₂PO₄, AR) were purchased from Beijing Chemical Factory. Water used in the experiments was purified using a Millipore water purification system. Saliva was collected from volunteers.

Instrumentation

The surface morphology and thickness of the polySBMA brushes and the IPN hydrogel film on the quartz chips were determined by atomic force microscopy (AFM) operated in a contact mode using a scattering SNOM (Neaspec GmbH). Attenuated total reflection-Fourier transform infrared spectra (ATR-FTIR) of the film surfaces were recorded using a Fourier-transform infrared spectrometer (Nicolet 560). X-ray photoelectron spectroscopy (XPS, ESCALAB250Xi) was used to quantitatively determine the elemental compositions, including nitrogen (N), sulfur (S), bromine (Br) and boron (B), of the surface of the material. The photoelectron take-off angle is 15°. The PBA-functionalized hydrogel film-coated and IPN hydrogel film-coated quartz chips were placed in saliva for 48 h at room temperature. The quartz chips were then rinsed with water and dried under a N₂ stream. Finally, the samples were coated with gold and then subjected to observation using a scanning electron microscope (Hitachi S-4800).

Synthesis of the IPN hydrogel film

Preparation of thiol-coated surfaces. First, quartz chips were sonicated in a Piranha solution (98% H₂SO₄ : 30% H₂O₂ = 7 : 3) for 10 min to eliminate organic substances and were thereafter rinsed with distilled water and dried under a N₂ stream. The cleaned quartz chips were then immersed in a 1×10^{-3} M ω-mercaptoundecyl bromoisobutyrate initiator solution by forming a self-assembled monolayer (SAM) at room temperature for 24 h. Before polymerization, the quartz chips were

coated with a SAM, rinsed with pure ethanol, and then dried under a N₂ stream.

Preparation of polySBMA brushes via surface-initiated ATRP. Ten milliliters of a mixture containing ethanol and distilled water (1 : 1; v/v) was degassed using three freeze–pump–thaw cycles. After that, it was transferred under a N₂ atmosphere to a Schlenk tube containing CuBr (19.1 mg, 133 μM), CuBr₂ (5.9 mg, 26.5 μM), and Me₄Cyclam (40.0 mg, 160 μM). In a separate Schlenk tube, a catalyst solution (blue solution) was mixed with a monomer SBMA (1500 mg, 5.4 mmol). The polymerization solution was then transferred to a reactor containing the quartz chips coated with a SAM. The polymerization reaction was carried out at 30 °C under a N₂ atmosphere, and the samples were withdrawn at different times to obtain polySBMA brushes with varying lengths. The quartz chips coated with polySBMA brushes were washed with ethanol, followed by water and were then stored in phosphate buffered saline (PBS).

Fabrication of IPN hydrogel films. First, a pre-polymer solution consisting of 25% PBA, 2% BIS, 71% AM, and 2% HMPP (by mass) in the DMSO solvent was prepared. After that, 25 μL of the prepared pre-polymer solution was deposited onto the upper electrode of polySBMA brush-coated quartz chips for 30 min, and then spun at a speed of 3500 rpm for 1 min. The coated quartz chips were subsequently irradiated with ultraviolet light ($\lambda = 365$ nm) under a N₂ atmosphere for 60 min for UV curing. Finally, the obtained IPN hydrogel film-coated quartz chips were repeatedly rinsed with ethanol, followed by distilled water. The zwitterionic hydrogel (z-hydrogel) film was prepared using a similar procedure, except that the pre-polymer solution consisted of 25 wt% PBA, 5 wt% SBMA, 2 wt% BIS, 66 wt% AM, and 2 wt% HMPP (by mass) in a solvent containing ethanol and distilled water (1 : 1 v/v) and was placed in uncoated quartz chips. The PBA-functionalized hydrogel film was also prepared using the same procedure, except that the quartz chips were uncoated.

Synthesis of pSBMA coating modified PBA-functionalized hydrogel film

The gold-coated PBA-functionalized hydrogel film was prepared by magnetron sputtering and was then immersed in a 1×10^{-3} M ω -mercaptoundecyl bromoisobutyrate initiator solution at room temperature for 24 h. After degassing using three freeze–pump–thaw cycles, 10 mL of ethanol/distilled water mixture (1 : 1 v/v) was transferred under a N₂ atmosphere to a Schlenk tube containing CuBr (19.1 mg, 133 μM), CuBr₂ (5.9 mg, 26.5 μM), and Me₄Cyclam (40.0 mg, 160 μM). In another Schlenk tube, the catalyst (blue solution) was mixed with the monomer SBMA (1500 mg, 5.4 mmol) and was then transferred to a reactor containing the PBA-functionalized hydrogel film coated with a SAM. The reaction was carried out at 30 °C under a N₂ atmosphere for 1 h, and the resultant polySBMA coating modified PBA-functionalized hydrogel film was washed with ethanol, followed by water, and then stored in phosphate buffered saline (PBS).

Verification of glucose sensitivity and protein resistance

A quartz chip coated with the IPN hydrogel film was dried under a N₂ stream and then installed in the flow cell of a QCM 200 system (fundamental frequency of 5 MHz). PBS (0.1 mol L⁻¹) was continuously pumped into the flow cell, during which the frequency of the quartz chip was real-time monitored using the QCM data acquisition software. The glucose detection capacity of the sensor was evaluated as follows: a solution (1 mL) containing increasing glucose concentration (in PBS) from 0 to 50 mg L⁻¹ or decreasing glucose concentration (in PBS) from 50 to 0 mg L⁻¹ was gradually pumped into the flow cell every 2 min, and the frequency shift ΔF associated with each glucose concentration was recorded. To investigate the effect of pH on the glucose sensitivity of the IPN hydrogel film, the experiments were conducted at different pH values from pH = 7.3 to pH = 7.8. To confirm the repeatability of the IPN hydrogel film, the glucose solution at concentrations of 0 and 10 mg L⁻¹, 30 mg L⁻¹ and 50 mg L⁻¹ were repeatedly pumped into the flow cell respectively. The protein resistance of the IPN hydrogel film was measured according to the above procedure.

Conclusions

In summary, the IPN hydrogel film was successfully fabricated by infiltrating the glucose-sensitive monomer into the zwitterionic polymer brush matrix. The IPN hydrogel film had excellent protein-resistant properties because of the strong hydration capacity of polySBMA brushes, which could reduce the adsorption of mucin by nearly 88%. Additionally, due to the presence of the stable hydration layer, the IPN hydrogel film enhanced glucose sensitivity with a value of nearly 2 fold compared to the PBA-functionalized hydrogel film. The IPN hydrogel film could also detect the typical salivary glucose level (0–50 mg L⁻¹) in diluted saliva with good response and recovery behavior. These results demonstrate that the IPN hydrogel film exhibits significant potential as an antifouling and sensitive glucose probe for the QCM sensor for non-invasive monitoring of glucose in saliva.

Conflicts of interest

There are no conflicts to declare.

Acknowledgements

This work is supported by the Science and Technology Service Network Project (STS Program) of Chinese Academy of Sciences (KFJ-STZ-ZDTP-063), the National Key Research and Development Program of China (2016YFA0201600), the Ministry of Science and Technology focused on the research of “early identification, early diagnosis and cutting point of diabetes risk factors” (2016YFC1305700), the Jiangsu Provincial

Basic Public Health Service Innovation Pilot Project (WDF15-967), and the Jiangsu Medical Device Industry Technology Innovation Center Joint Fund (SYC2018004).

Notes and references

- 1 S. Wild, C. Roglic, A. Green, R. Sicree and H. King, *Diabetes Care*, 2004, **27**, 1047–1053.
- 2 D. C. Klonoff, L. Blonde and G. Cembrowski, *J. Diabetes Sci. Technol.*, 2011, **5**, 1529–1548.
- 3 I. Mamkin, S. Ten, S. Bhandari and N. Ramchandani, *J. Diabetes Sci. Technol.*, 2008, **2**, 882–889.
- 4 M. C. Torjman, N. Dalal and M. E. Goldberg, *J. Diabetes Sci. Technol.*, 2008, **2**, 178–181.
- 5 B. W. Barry, *Eur. J. Pharm. Sci.*, 2001, **14**, 101–114.
- 6 P. Abikshyeet, V. Ramesh and N. Oza, *Diabetes, Metab. Syndr. Obes.: Targets Ther.*, 2012, **5**, 149–154.
- 7 Y. H. Chen, S. Y. Lu, S. S. Zhang, Y. Li, Z. Qu, Y. Chen, B. W. Lu, X. Y. Wang and X. Feng, *Sci. Adv.*, 2017, **3**, e1701629.
- 8 S. K. Vashist and P. Vashist, *J. Sens.*, 2011, **1**, 2011.
- 9 T. Zhou, K. A. Marx, M. Warren, H. Schulze and J. Braunschut, *Biotechnol. Prog.*, 2000, **16**, 268–277.
- 10 R. E. Speight and M. A. Cooper, *J. Mol. Recognit.*, 2012, **25**, 451–473.
- 11 C. Yao, T. Zhu, Y. Qi, Y. Zhao, H. Xia and W. Fu, *Sensors*, 2010, **10**, 5859–5871.
- 12 K. A. Marx, *Biomacromolecules*, 2003, **4**, 1099–1120.
- 13 M. Lazerges, H. Perrot, N. Rabehagaso and C. Comepere, *Biosensors*, 2012, **2**, 245–254.
- 14 Y. Tsuge, Y. Moriyama, Y. Tokura and S. Shiratori, *Anal. Chem.*, 2016, **88**, 10744–10750.
- 15 D. D. Erbahar, I. Gurol, F. Zelder and M. Harbeck, *Sens. Actuators, B*, 2015, **207**, 297–302.
- 16 C. Li, X. Chen, F. Y. Zhang, X. X. He, G. Z. Fang, J. F. Liu and S. Wang, *Anal. Chem.*, 2017, **89**, 10431–10438.
- 17 Q. Dou, D. B. Hu, H. K. Gao, Y. M. Zhang, A. K. Yetisen, H. D. Butt, J. Wang, G. J. Nie and Q. Dai, *RSC Adv.*, 2017, **7**, 41384–42390.
- 18 A. Hucknall, S. Rangarajan and A. Chilkoti, *Adv. Mater.*, 2009, **21**, 2441–2446.
- 19 S. Jiang and Z. Cao, *Adv. Mater.*, 2010, **22**, 920–932.
- 20 C. Rodriguez and A. B. Alles, *Langmuir*, 2009, **25**, 6328–6333.
- 21 J. Ladd, Z. Zhang, S. Chen, J. C. Hower and S. Jiang, *Biomacromolecules*, 2008, **9**, 1357–1361.
- 22 S. H. Baxamusa and K. K. Gleason, *Adv. Funct. Mater.*, 2009, **19**, 3489–3496.
- 23 G. R. Hendrickson, M. H. Smith, A. B. South and L. A. Lyon, *Adv. Funct. Mater.*, 2010, **20**, 1697–1712.
- 24 S. Herrwerth, W. Eck, S. Reinhardt and M. Grunze, *J. Am. Chem. Soc.*, 2003, **125**, 9359–9366.
- 25 J. M. Wang, H. Sun, J. J. Li, D. Y. Dong, Y. B. Zhang and F. L. Yao, *Carbohydr. Polym.*, 2015, **117**, 384–391.
- 26 R. L. Carr, B. Y. Zhou, J. E. Karuse, H. Xue and S. Jiang, *Biomaterials*, 2011, **32**, 6893–6899.
- 27 Y. H. Zhu, X. W. Xu, N. D. Brault, A. J. Keefe, X. Han, Y. Deng, J. Q. Xu, Q. M. Yu and S. Y. Jiang, *Anal. Chem.*, 2014, **86**, 2871–2875.
- 28 Y. C. Hu, B. Liang, L. Fang, G. L. Ma, G. Yang, Q. Zhu, S. F. Chen and X. S. Ye, *Langmuir*, 2016, **32**, 11763–11770.
- 29 P. F. Ren, Y. Fang, L. S. Wan, X. Y. Ye and Z. K. Xu, *J. Membr. Sci.*, 2015, **486**, 195–206.
- 30 T. Xiang, T. Lu, Y. Xie, W. F. Zhao, S. D. Sun and C. S. Zhao, *Acta Biomater.*, 2016, **40**, 162–171.
- 31 D. Rana and T. Matsuura, *Chem. Rev.*, 2010, **110**, 2448–2471.
- 32 J. S. Rio, O. Y. Henry, P. Jolly and D. E. Ingber, *Nat. Nanotechnol.*, 2019, **14**, 1143–1149.
- 33 Y. F. Yue, M. A. Haque, T. Kurokawa, T. Nakajima and J. P. Gong, *Adv. Mater.*, 2013, **25**, 3106–3110.
- 34 K. G. Noh and S. Y. Park, *Adv. Funct. Mater.*, 2018, **28**, 1707562.
- 35 J. E. Stumpel, E. R. Gil, A. B. Spoelstra, W. M. Cees, D. J. Bastiaansen, D. J. Broer and P. H. J. Albertus, *Adv. Funct. Mater.*, 2015, **10**, 3314–3320.
- 36 S. Park, S. Edward, S. J. Hou, R. Boudreau, R. Yee and K. J. Jeong, *Biomater. Sci.*, 2018, **7**, 1276–1280.
- 37 W. Xiao, J. He, J. W. Nichol, L. Wang, C. B. Hutson, B. Wang, Y. Du, H. Fan and A. Khademhosseini, *Acta Biomater.*, 2011, **7**, 2384–2393.
- 38 S. Liu and W. W. Guo, *Adv. Funct. Mater.*, 2018, **28**, 1800596.
- 39 S. Kim, J. Moon, J. S. Chol, W. K. Cho and S. M. Kang, *Adv. Funct. Mater.*, 2016, **26**, 4099–4105.
- 40 X. Wang, Y. Wang, S. Bi, Y. G. Wang, X. G. Chen, L. Y. Qiu and J. Q. Sun, *Adv. Funct. Mater.*, 2014, **24**, 403–411.
- 41 Z. Zhang, S. Chen, Y. Chang and S. Jiang, *J. Phys. Chem. B*, 2006, **110**, 10799–10804.
- 42 L. Mi and S. Jiang, *Angew. Chem., Int. Ed.*, 2014, **53**, 1746–1754.
- 43 Y. Chang, S. F. Chen, Z. Zhang and S. Jiang, *Langmuir*, 2006, **22**, 2222–2226.
- 44 Z. Zhang, T. Chao, S. F. Chen and S. Jiang, *Langmuir*, 2006, **22**, 10072–10077.
- 45 C. R. Emmenegger, E. Brynda, T. Riedel, M. Houska, V. Subr, A. B. Alles, E. Hasan, J. E. Gautrot and W. T. S. Huck, *Macromol. Rapid. Commun.*, 2011, **32**, 952–957.
- 46 A. Hucknall, D. H. Kim, S. Rangarajan, R. T. Hill, W. M. Reichert and A. Chilkoti, *Adv. Mater.*, 2009, **18**, 1968–1971.
- 47 C. Zhang, M. D. Losego and P. V. Braun, *Chem. Mater.*, 2013, **25**, 3239–3250.
- 48 Z. Z. Zhang, Q. Dou, S. W. Wang, D. B. Hu, X. D. Guo, B. X. Liao, Z. P. Zhao, H. L. Liu and Q. Dai, *J. Mater. Chem. C*, 2020, **8**, 9655–9662.
- 49 P. S. Liu, Q. Chen, S. S. Wu, J. Shen and S. C. Lin, *J. Membr. Sci.*, 2010, **350**, 387–394.

- 50 A. Carlamark and E. Malmstrom, *Biomacromolecules*, 2003, **4**, 1740–1745.
- 51 M. V. Beek, L. Jones and H. Sheardown, *Biomaterials*, 2008, **29**, 780–789.
- 52 R. J. Ma and L. Q. Shi, *Polym. Chem.*, 2014, **5**, 1503–1518.
- 53 D. Shen, H. J. Yu, L. Wang, A. Khan, F. Haq, X. Chen, Q. Huang and L. S. Teng, *J. Controlled Release*, 2020, **321**, 236–258.
- 54 A. M. Horgan, A. J. Marshall, S. J. Kew, K. E. S. Dean, C. D. Creasey and S. Kabilan, *Biosens. Bioelectron.*, 2006, **21**, 1838–1845.
- 55 K. Ngamchuea, K. Chaiswamongkhol, C. B. Mcauley and R. G. Compton, *Analyst*, 2018, **143**, 81–99.
- 56 S. H. Baxamusa and K. K. Gleason, *Adv. Funct. Mater.*, 2009, **19**, 3489–3496.
- 57 E. F. Irwin, J. E. Ho, S. R. Kane and K. E. Healy, *Langmuir*, 2005, **21**, 5529–5536.
- 58 M. S. Lin, C. C. Liu and C. T. Lee, *J. Appl. Polym. Sci.*, 1998, **72**, 585–592.
- 59 Z. X. Zhang, Q. Dou, H. K. Gao, B. Bai, Y. M. Zhang, D. B. Hu, A. K. Yetisen, H. D. Butt, X. X. Yang, C. J. Li and Q. Dai, *Adv. Healthcare Mater.*, 2018, **7**, 1700873.
- 60 Q. Dou, Z. F. Zhang, Y. X. Wang, S. W. Wang, D. B. Hu, Z. P. Zhao, H. L. Liu and Q. Dai, *ACS Appl. Mater. Interfaces*, 2020, **12**, 34190–34197.
- 61 Y. Yao, X. D. Chen, H. H. Guo and Z. Q. Wu, *Appl. Surf. Sci.*, 2011, **257**, 7778–7782.
- 62 X. Chen, J. Chen, F. B. Wang, X. Xiang, M. Luo, X. H. Ji and Z. K. He, *Biosens. Bioelectron.*, 2012, **35**, 363–368.
- 63 A. Heller and B. Feldman, *Chem. Rev.*, 2008, **108**, 2482–2505.
- 64 W. J. Zhang, Y. Q. Du and M. L. Wang, *Sens. Bio-Sens. Res.*, 2015, **4**, 23–29.
- 65 E. Hartl, N. Dixit, A. Besheer, D. Kalonia and G. Winter, *Eur. J. Pharm. Biopharm.*, 2013, **85**, 781–789.